

# 3D printing of hydrogels and nanoparticle containing bio-inks for bone tissue regeneration

Abeer Barakat

*Dr. Jose Manuel Garcia-Torres*

*Prof. Maria Pau Ginebra*

*Materials Science and Metallurgical Engineering Department, Universitat Politècnica de Catalunya*

**Abstract**—In tissue engineering, biomaterials paves the route for faster and less painful regeneration of tissues. In the present study, 2 set of scaffolds made of mixtures of different proportions of low and medium molecular weight alginates with and without hydroxyapatite nanoparticles (HA NPs) were prepared by 3D printing for bone regeneration. Different tests were done to characterize the scaffolds. Printability of scaffolds, SEM analysis were performed to characterize printed scaffolds of the desired design. Biodegradation studies of the scaffolds as well as cell viability in 3D culture were performed. All the formulations with different alginates proportions (with and without HA NPs) were printable. SEM showed the intact scaffold with well-defined filaments showing porous spongy structure with homogeneously distributed components. Biodegradation analyses showed complete degradation of the scaffolds within 14 to 21 days depending on the composition. Cell viability analysis revealed 95 to 100% viability of cells after 28 days.

**Index Terms**—Nano-biotechnology: 3D bio-printing, biomaterials, tissue engineering, bone regeneration.

## I. INTRODUCTION

TISSUE Engineering (TE) is a scientific field mainly focused on the development of tissue and organ substitutes by controlling biological, biophysical and/or biomechanical parameters in the laboratory [1]. It combines the principles of cell transplantation, material science, and bioengineering and it is one of the applications used in the field of regenerative medicine replacing damaged tissues by synthetic biocompatible tissue matrices. They are usually prepared by manufacturing artificial scaffolds, or by removing cellular components from tissues via mechanical and chemical manipulation to produce collagen-rich matrices. These matrices tend to slowly degrade after implantation and are generally replaced by the extracellular matrix (ECM) proteins that are secreted by host cells infiltrating the matrix [2]. This field is becoming very useful in the study of human physiology and physiopathology as well as cytotoxicity testing model for personalized medicine. Many trials were made using this technology to replace or regenerate a whole organ or just a tissue graft as in bone, cartilage and wound healing.

Current techniques to produce engineered bone tissue constructs result in stiff, rigid scaffolds with limited plasticity and ability to form irregular architectures. Another limitation is the relatively poor spatial control of the distribution of cells, matrix components and bioactive cues within the engineered

construct for enhanced uniform healing. One way to overcome the previous limitations is through the use of emerging additive manufacturing strategies. In particular, 3D bio-printing has evolved as a promising technique to fabricate complex scaffold geometries able to mimic aspects of the composition and organisation of native tissues through the simultaneous deposition of biomaterials, cells, and/or proteins in defined locations. 3D printing is influenced by two main factors: the technique used and the bio-ink selected. On one hand and according to Lee et al. [3], 3D printing technology falls in the six following categories: Binder Jetting (BJ), Direct Energy Deposition (DED), Material Extrusion (ME), Powder bed fusion (PBF), Sheet Lamination (SL) and Vat photopolymerization (VP). Among them, ME is one of the most widely employed because it allows developing 3D structures under mild conditions (e.g. room temperature) which is crucial for the incorporated cells to stay viable [4]. On the other hand, a proper selection of the bio-ink composition is a big challenge as the material not only should provide mechanical and structural support, but also protect the cells from damage during printing and ultimately favor cell adhesion and promote cell proliferation.

Currently, the most widely investigated materials for 3D bio-printing are hydrogels due to their inherent properties. They have high water content and show an interwoven structure that mimic that of the natural extracellular matrix rendering them favorable for live cell incorporation. Moreover, they can be easily functionalized or modified to replicate the physicochemical properties of most biological tissues [5]. These unique features make hydrogels excellent environments for cell attachment and proliferation within their hydrated hydrogel networks, which offer abundant space for cell growth while facilitating the transportation of essential metabolites and nutrients to the encapsulated cells [6]-[8]. The hydrogels are also used to deliver drugs [9],[10], DNA or RNA fragments, sustained release for medications, angiogenic and growth factors and they offer a major role in pharmaceutical and tissue engineering fields [11]-[13].

Alginate is a common natural biopolymer used in 3D bio-printing as it is highly biocompatible, shows wide pore size distribution and their physical properties can be potentially tailored to improve their performance for tissue regeneration. One suitable way to modify the alginate properties is by preparing hydrogel composites through incorporating other hydrogels or nanomaterials like hydroxyapatite nanoparticles

(HA NPs) [6], [14]. Hydroxyapatite is a crystal structure similar to inorganic component of natural bones. Biological HA comprises 7% of the natural bone extracellular matrix. It can be reabsorbed into the bone tissue and increase the rate of bone regeneration due to its osteo-inductive effect. Moreover, the interpenetration between two polymer networks or the physical interaction of inorganic nanoparticles with the matrix enhances the mechanical properties of the composite. Scaffold stiffness have been shown to have a key role in cell adhesion, proliferation and differentiation, property that can be modulated by the molecular weight of the alginate source, the choice of cross-linker and the gelling time, or the incorporation of nanoparticles into the alginate. The design of this study is based on former studies which served to create scaffolds for bone tissue regeneration using 3D printing [15]-[18].

In the present work, a novel study consisting of mixtures of 2 different molecular weight alginates were used to prepare bio-inks for the 3D printing of scaffold for bone tissue regeneration. The use of different proportions of low and medium molecular weight alginates will allow modifying the properties of the hydrogel looking for a formulation that can host cells with high viability. Printability, morphology, biodegradation and cell viability were tested for all formulations. After that, HA NPs were incorporated into the alginate hydrogel aiming to impart a double role: (i) to improve the stability of the hydrogel and (ii) to favour bone regeneration as hydroxyapatite is the main component of natural bone tissue. The same tests were performed onto the alginate-based scaffolds containing variable amounts of HA NPs in addition to characterization of HA NPs.

## II. MATERIAL AND METHODS

Preparation of bio-inks. Inks were prepared using two sodium alginate powders of varying molecular weight (Low viscosity: 216.121 g/mol, Sigma Aldrich and medium viscosity: 600.000 g/mol, ITW reagents), Pluronic F-127 (Poloxamer 407, Sigma Aldrich), hydroxyapatite nanoparticles (HA NPs) (see synthesis procedure below) and deionized water as medium. First, five inks (F1-F5) were prepared by mixing different proportion of the two MW alginates with a fixed amount of Pluronic. After that, F2 was modified by adding different amounts of hydroxyapatite nanoparticles. Tables I and II summarize the composition of the two sets of inks. The inks were prepared by mixing the two alginates, pluronic, HANPs (when needed) and deionized water using a speed mixer (Hauschild engineering) to assure homogeneous distribution of all the components.

Printing process: Using 3D printing machine and a g-code, especially designed to create the desired conformation, the

hydrogels are printed into a 3d scaffolds (10 mm in diameter and 4 mm in height). The printing process was manipulated by controlling the speed of printing and the flow rate by material extrusion followed by ionic cross linking, which is done by replacing the univalent Na<sup>+</sup> of sod-alginates by divalent Ca<sup>2+</sup> ions by the soaking of the scaffolds in 150 mM Ca Cl<sub>2</sub> for 10 min. Calcium ions forms bonds between the chains of alginates producing a stable mesh of Ca-alginates.

Cell incorporation: Saos-2 (Osteo-sarcome stem cells) cells were incorporated into the inks in order to study cell viability of the scaffolds. Some considerations were taken into account when preparing the bio-inks. First, all the chemicals were sterilized using either oxygen plasma (Alginates, Pluronic) for 10 min (Electronic diener plasma, Germany), or using autoclave (HA NPs) at 121 °C for 2 hours (JP Selecta). Second, supplemented Mc Coy's medium was used to replace distilled water. This supplemented medium was prepared by mixing 35 mL of Mc Coy's culture media (SigmaAldrich) with 5 mL fetal bovine serum (Gibco), 0.5 mL penicillin/streptomycin antibiotic (Gibco), 1 mL HEPES (Gibco), 0.5 mL L-Glutamine (Gibco) and 0.5 mL sodium pyruvate (Gibco). Saos-2 cancer stem cells were cultured for 4 days at 37 °C and 5 % CO<sub>2</sub> before bio-ink preparation and printing. Seeding density of the bio-ink was of 5 × 10<sup>6</sup> cells/g. After printing, Supplemented Mc Coy's medium was used to nourish cells by replacement of 2 mL of media per scaffold every 48 days.

Preparation of HANPs. Hydroxyapatite nanoparticles were prepared according to Zhao et al. [19]. Briefly, 0.2 M H<sub>3</sub>PO<sub>4</sub> (Sigma Aldrich) solution was added at 1 ml/min to 2.475 g of CaOH dissolved in 100 ml of distilled water. The CaOH solution was kept at 40 °C and under magnetic stirring (700 rpm). The pH was monitored and the reaction was stopped at pH 8. After that, HANPs were precipitated and washed 5 times with distilled water. The pellet was then freeze dried for 4 hours and lyophilized overnight (Telsatar). HANPs were re-suspended in a 10 mL of 0.2 M sodium citrate tribasic hydrate (Sigma Aldrich) solution, sonicated using digital sonifier (Branson) to prevent nanoparticles aggregation.

Material Characterization. The morphology, structure and architecture of the 3D printed hydrogel scaffolds were observed using an SEM (Phenom world, Thermofisher scientific) at an accelerated voltage of 10 kV. The scaffolds were freeze-dried in a freeze-drying machine (TELSTAR) in order to remove the water content. Before being mounted on aluminum stubs, they were sputtered with carbon. Energy dispersive spectroscopy (EDS) coupled with SEM was used to detect and map the distribution of hydroxyapatite into the scaffolds. Transmission Electron Microscopy (TEM, JEOL 1010) was used to characterize the size and shape of the HA NPs. The nanoparticles were drop casted onto a carbon coated

**Table I**  
COMPOSITION OF THE INKS CONTAINING THE TWO ALGINATES AND PLURONIC.

| Formulation | Medium viscosity alginate % (w/w) | Low viscosity alginate % (w/w) | PluronicF-1 27 (w/w) % | Distilled water (w/w) % |
|-------------|-----------------------------------|--------------------------------|------------------------|-------------------------|
| F1          | 0                                 | 8                              | 13                     | 79                      |
| F2          | 2                                 | 6                              | 13                     | 79                      |
| F3          | 4                                 | 4                              | 13                     | 79                      |
| F4          | 6                                 | 2                              | 13                     | 79                      |
| F5          | 8                                 | 0                              | 13                     | 79                      |

**Table II**  
COMPOSITION OF THE INKS CONTAINING HYDROXIAPPATITE NNOPARTICLES.

| Formulation | Medium viscosity alginate (w/w) % | Low viscosity alginate (w/w) % | Pluronic F-127 (w/w) % | HANPs (w/w) % | Distilled water (w/w) % |
|-------------|-----------------------------------|--------------------------------|------------------------|---------------|-------------------------|
| F2/HA 0.5 % | 2.0                               | 6.0                            | 13.0                   | 0.5           | 78.5                    |
| F2/HA 1 %   | 2.0                               | 6.0                            | 13.0                   | 1.0           | 78.0                    |
| F2/HA 2 %   | 2.0                               | 6.0                            | 13.0                   | 2.0           | 77.0                    |
| F2/HA 3 %   | 2.0                               | 6.0                            | 13.0                   | 3.0           | 76.0                    |
| F2/HA 4 %   | 2.0                               | 6.0                            | 13.0                   | 4.0           | 75.0                    |
| F2/HA 5 %   | 2.0                               | 6.0                            | 13.0                   | 5.0           | 74.0                    |

copper grid from a sodium citrate suspension. Structural characterization of hydroxyapatite was performed by X-ray diffraction (XRD) using a diffractometer (Bruker Corp.) equipped with a Cu K $\alpha$  anode operated at 40 kV and 40 mA. Data were collected in 0.02  $^{\circ}$  steps over the 2 $\theta$  range of 10–60 $^{\circ}$  with a counting time of 2s per step. Phase identification was accomplished by comparing the experimental patterns to those of hydroxyapatite (JCPDS 09-0432). Fourier-transform infrared spectroscopy (FTIR) was used to detect the presence of the different polymeric components into the scaffold over time. Two scaffolds were prepared; one directly after printing and another after soaking in PBS for one day were freeze-dried and lyophilized then tested using FTIR (Nicolet 6700, Thermo, IET). The spectra represent an average of 64 scans, collected in the range 450 to 4000 cm $^{-1}$  at a resolution of 4 cm $^{-1}$ .

Degradation of scaffolds. Degradation analysis was performed by immersing of scaffolds in PBS solution at 37 oC. The scaffolds were weighed before and after lyophilization at days 1, 3, 7, 14, 21 and 28 compared to the initial weight at day 0. The degradation was described in term of mass swelling (q) and mass loss with time calculated from the following equations [20]:

$$q = \frac{m_{swollen}}{m_{dry}} \quad (1)$$

$$Actual\ macromer\ fraction = \frac{m_{dry, t=0}}{m_{initial, t=0}} \quad (2)$$

$$m_{initial, dry} = m_{initial} \times actual\ macromer\ fraction \quad (3)$$

$$Mass\ loss = \frac{m_{initial, dry} - m_{dry}}{m_{initial, dry}} \times 100 \quad (4)$$

Where  $m_{initial, t=0}$  is the weight of the scaffold right after printing,  $m_{dry, t=0}$  is the weight of the scaffolds after printing and lyophilization without degradation,  $m_{swollen}$  is the weight of the scaffold after submerging in PBS without lyophilization,  $m_{dry}$  the weight of the scaffold after immersing in PBS and lyophilization. The amount of weight loss was directly proportional to the amount of degradation of the scaffolds with time.

**Live/Dead cell assay.** Cell-laden scaffolds were rinsed in sterile PBS and then stained in 1ml of propidium iodide (PI) and calcein solution (20  $\mu$ l of PI+ 5 ml of calcein in 10  $\mu$ l PBS) for 20 min. After washing in PBS, they were fixed in 1 ml of 4% paraformaldehyde (2.5 mL 16% paraformaldehyde + 7.5 mL PBS) for 20 min and washed again with PBS [21]. Finally, 1 ml of DAPI stain solution was added (10  $\mu$ l of DAPI in 10 mL of PBS) for 1 min and washed with PBS. Afterwards, scaffolds were imaged with Confocal Laser Scanning Microscope (Zeiss 800) at 488 and 543 nm channels. Three images per scaffold were captured at different days (3, 7, 14, 21 and 28 days). Cell viability by manual count and cell circularity estimation using Image-J software were performed.

### III. RESULTS AND DISCUSSION

#### A. Alginate-pluronic hydrogel scaffolds

The prepared bio-inks consisting of alginates/pluronic (F1-F5) were excellent for extrusion-based 3D printing through adjusting the printing parameters including printing speed and flow rate. These formulations were assessed on the continuity of the gel strands as extruded through the needle as well as by the shape fidelity of the printed scaffolds. Images of the printed inks into scaffolds 1.0 cm in diameter are seen in Fig. 1a. The inks were viscous enough to maintain separate and continuous lines and therefore avoid spreading. Moreover, all formulations were able to support consecutive and distinct layers keeping porosity and shape fidelity to the CAD scaffold design. Thus, all the formulations were successfully printed as they are able to keep the structural integrity without

deformation and collapse due to the sufficient strength. The printed scaffolds showed a slight change from translucent to opaque after immersion in 150 mM  $\text{CaCl}_2$  and due to the crosslinking of the alginate chains.

After that, a more detailed analysis of the morphology of the scaffolds was performed by SEM. Figure 1b shows representative SEM images of the 3D printed formulations after freeze drying. As it can be observed, all the scaffolds show well-defined and self-supporting filaments with thicknesses ranging from 250 to 375  $\mu\text{m}$ , approximately. The difference with the nozzle diameter is because the samples shrink after water removal by freeze drying. On the other hand, some microporosity is observed into the filaments which is attributed to the dissolution of pluronic, a water-soluble polymer (Fig. 1c). The mean pore size was different between formulations, ranging from 20 to 45  $\mu\text{m}$ . While the scaffolds of F1 showed the highest pore size, it decreased in the rest of the formulations, probably attributed to the presence of the alginate with higher MW that forms a denser network. It is expected this microporosity will benefit cell-laden scaffolds as it will allow the access of nutrients to the embedded cells.

In order to verify the presence of the polymeric components into the scaffold, FTIR analysis was performed. Figure 2a shows the FTIR spectra of the as-printed scaffolds and after being stored for 1 day in  $\text{CaCl}_2$  solution. The spectrum of the as-printed scaffolds shows peaks characteristics of alginate and pluronic (Fig. 2a, curve I). Alginate displays characteristic bands denoting asymmetric and symmetric stretching of  $-\text{COO}$  modes found at 1595 and 1410  $\text{cm}^{-1}$ , respectively; and C-O stretching vibration modes at 1080  $\text{cm}^{-1}$ . On the other hand, pluronic shows distinctive peaks at 2800, 1300 and 1110  $\text{cm}^{-1}$  attributed to C-H, C-C and C-O stretching vibration modes, respectively. However, the peaks corresponding to pluronic are no longer present after 1 day being stored in  $\text{CaCl}_2$

solution because it is dissolved off the scaffold (Fig. 2a, curve II). These results are in agreement with those found in the literature [22]-[25].

Degradability is another critical property of hydrogel scaffolds used for tissue engineering approaches. Thus, when the degradation is too fast, the scaffold loses its role of support for cells. In contrast, when the degradation rate is too slow, it would impede the emergence of new tissue. Figures 2b,c show the swelling ratio and the mass loss profiles over time for the scaffolds prepared from the formulations F1 to F5. As it can be observed, the mass loss for the different scaffolds is affected by their composition. Thus, formulations with higher low MW alginate contents (F1, F2) experience a higher water uptake resulting in a higher mass swelling; meanwhile, those formulations with a higher content of medium MW alginate (F3-F5) results in a lower mass swelling. The same trend has been observed when analyzing the mass loss profiles for the different formulations. The presence of a higher amount of the low MW alginate (F1, F2) results in a higher mass loss over time. The scaffolds are completely degraded after 14 days of incubation. On the other hand, as the content of the medium MW alginate increases (F3-F5), the degradation rate is reduced over time and they were not completely degraded till 21 days after incubation. These results can be explained by differences in the crosslinking density of low and medium MW alginates and their mixtures. Thus, the higher the MW, the higher the number of bonds and therefore the higher the compactness of the filaments hindering degradability. These results are also in agreement with differences in the microporosity observed by SEM. Microporosity was higher in the scaffolds with higher content of the low MW alginate, thus favoring scaffold degradation. We can conclude that the scaffold composition has a significant effect on the degradability. It is advantageous as it allows tuning the degradation rate and synchronize it with the natural tissue growth, so the cells would be attached to the natural ECM produced by body to regenerate tissue in the injured area and replace the synthetic scaffolds.

Finally, cell viability of the cell-laden scaffolds was studied for the different inks prepared (F1-F5). Saos-2 cells were successfully encapsulated into the different inks and 3d printed into scaffolds showing high shape fidelity. Thus, neither the cell culture media nor the cell suspension modifies the printability of the different formulations. Cell viability was assessed after printing over a period of 28 days by optical observation and count of live and dead cells. Scaffolds were kept in supplemented cell culture medium to provide with nutrients to the cells during this period. It is worth mentioning that this live/dead estimation method is a semi-quantitative analysis as the number of cells cannot be controlled during the whole culture time due to lysis of dead cells with time and some loss of a fraction of cells from scaffolds due to continuous addition and removal of culture media especially with scaffold degradation. Metabolism and/or RNA analysis methods are recommended for better estimation.

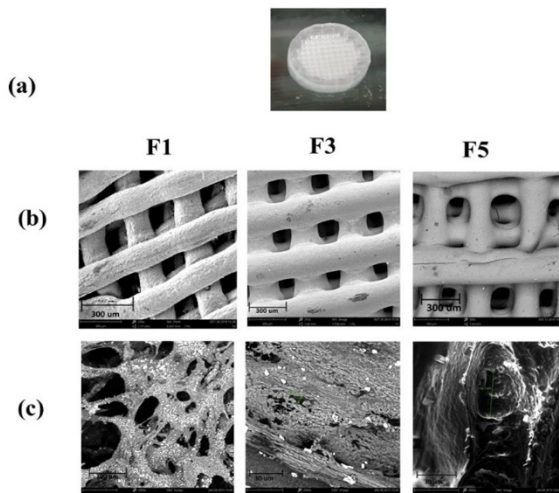


Fig. 1. (a) Optical image of a 3D printed scaffold from ink F1. (b) SEM images and (c) higher magnification SEM images of scaffolds obtained from F1, F3 and F5.

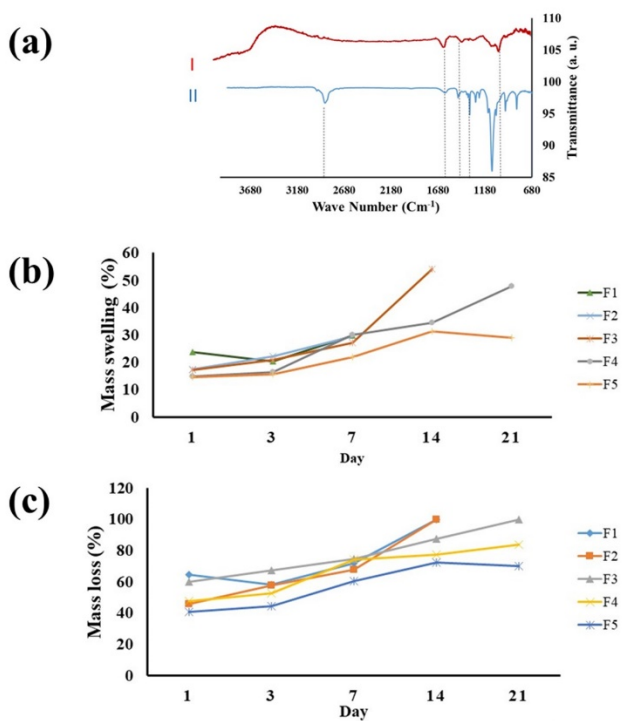


Fig. 2. (a) FTIR spectra for printed scaffold. (b) Mass swelling and (c) Mass loss ratio profiles for the scaffolds prepared using formulations F1-F5

As it can be observed in Fig. 3b, 3 days after incubation cell viability was higher (in the range 60-80%) in the scaffolds printed from inks with a higher content of low MW alginate. However, cell viability was lower (approximately 20%) in formulations F4 and F5. This low cell viability could be related to other factors such as: (i) the cells experience a higher shear stress during printing because of the higher viscosity of F4 and F5 inks, (ii) the cells experience an additional stress due to the higher contraction of the scaffolds with a higher content of medium MW alginate as a result of a higher crosslinking (iii), cell population contained a fraction of dead cells before printing, or (iv) the cells are affected by the cross linking agent. However, cell viability rises with time for the different scaffolds reaching around 90% in the scaffolds printed from inks F2, F3 and F4. Finally, after 28 days of incubation, scaffold from F4 had nearly 100% cell viability and that from F5 shows around 90% cell viability. It seems that the surviving cells still have the potential to recover and proliferate by further incubation in vitro, which will be investigated in future studies.

Cell circularity analysis using image J program revealed no differences between the different scaffolds and over time. Circularity of the cells was in the range of 0.4 to 0.6. It is worth mentioning that the value “1” indicates completely circular cells (less attached to the substrate) and value less than “1” indicates less cell circularity (more attached to the substrate).

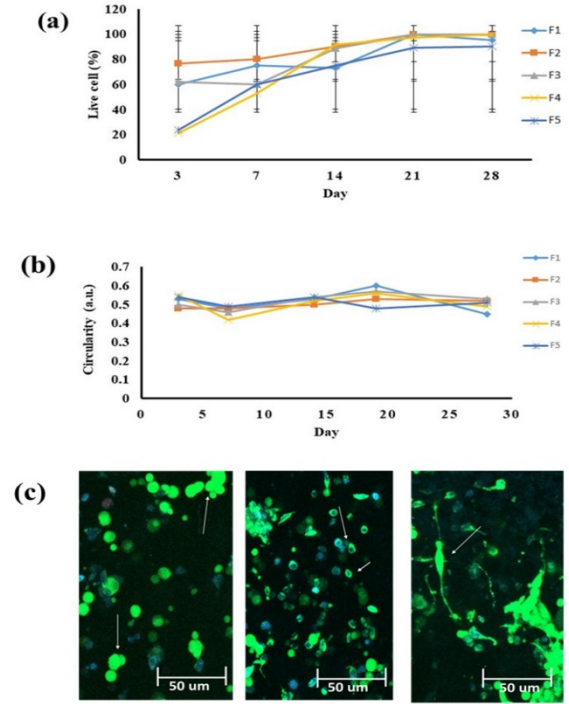


Fig. 3. (a) Graph showing the percentage of cell viability, (b) Graph showing the circularity of cell; in scaffolds of alginates without HA NPs, (c) Different types of cell morphology: (left) big dividing, (middle) small oval (right) very flat with pseudopodia.

Morphological observation of cells showed 3 types of cells (Fig. 3c): (i) big intensely green stained with no defined nucleus, (ii) small oval with big well-defined acentric nucleus and (iii) flattened cells with extended pseudopodia. At the beginning of cell culture (up to 7 days), scaffolds from F1 and F2 bio-inks showed bigger cells and a higher number of cells (type i) in comparison to the rest of the formulations. However, after the 7th day of culture, more cells of (type i) were observed in F3, F4 and F5 scaffolds. The observation of this type of cells (ii) could be related to the degradation of scaffolds with more compact structure allowing more space for cell growth.

More flattened cells (type iii) were observed at day 28 in F3, F4 and F5 than F1 and F2, especially in F5, that could be due to the more rigid substrate that these formulations provide due to less degradation with time compared to F1 and F2 with fast degradation. That contradicts with circularity analysis by image J processing because the flattened cells were in batches and the program cannot distinguish them as separate entities, this is why the photos had to be optically observed and assessed.

Although cells can be encapsulated in alginate, it has been reported that it has limited interactions with cells unlike native extracellular matrix. Interaction with the matrix is needed for

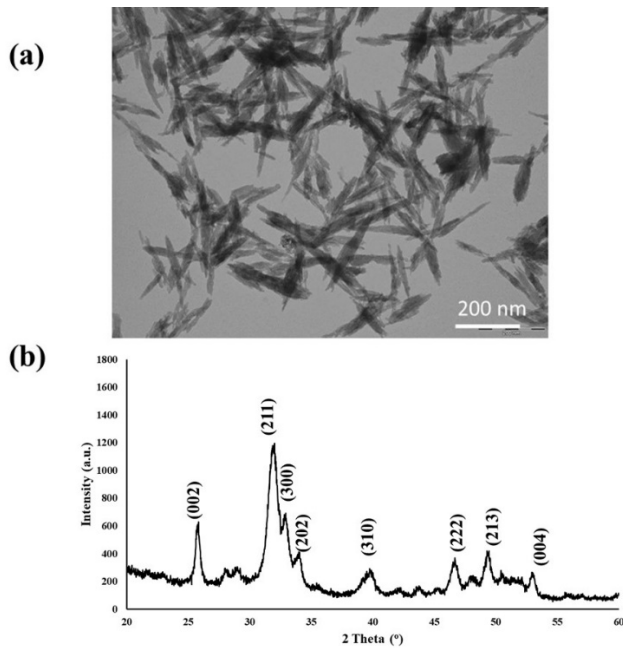


Fig. 4. (a) TEM micrograph of HA NPs, (b) XRD spectrum for HA NPs

the cells to proliferate, differentiate and begin new tissue formation. In order to promote cell adhesion, hydroxyapatite nanoparticles will be added into the alginate scaffolds. Moreover, the addition of HA NPs may have a second role: to improve the stiffness of the scaffolds [26].

### B. Alginate-pluronic-HA NPs hydrogel scaffold

Figure 4a shows a transmission electron microscopy image of the synthesized particles. They are characterized by a needle-shape morphology with a particle size around 200 nm. XRD of these nanoparticles clearly reveals the presence of the hydroxyapatite (Fig. 4b).

After the synthesis and characterization of the HA NPs, they were incorporated into the ink F2 (6 wt.% low MW alginate + 2 wt.% medium MW alginate) and 3D printed. We selected this ink because we observed the highest cell viability during the first 14 days of incubation compared to the other scaffolds. Different amounts of HA NPs (0.5-5 wt.%) were incorporated into the inks to study their effect on the scaffold properties.

Once the inks were prepared, their printability was evaluated. Again, we observed that all the HA NPs-containing inks allowed obtaining continuous and well-defined strands. Moreover, the scaffolds were self-supportive with good shape fidelity keeping the structural integrity without collapsing [15]-[18], [26]. Only formulation with 5% HA NPs showed more soft texture before cross-linking. SEM characterization allows observing well-defined and self-supporting filament with thicknesses ranging from 250 to 400  $\mu\text{m}$  (Fig. 5a). Again, some microporosity was observed in the HA NPs-containing scaffolds but with a bigger pore size than in HA free constructs (Fig. 5b). Finally, the distribution of the

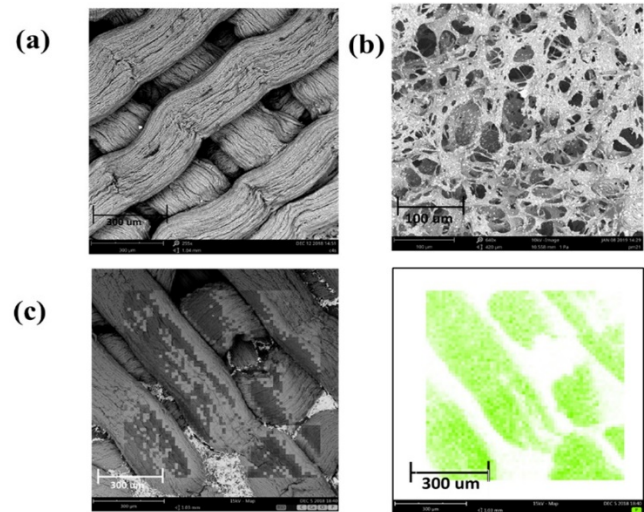


Fig. 5. SEM micrograph of 3D printed scaffolds (a) SEM Day 0, (b) SEM micrograph at day 1, (c) SEM-EDX analysis map for the scaffold with 0.5% HA. (left) The whole scaffold. (right) for Phosphorus.

HA NPs into the scaffolds was evaluated by EDS. Figure 4b shows the XRD pattern of the as-prepared nanoparticles. The peaks in the diffractogram clearly fit with the standard peaks for hydroxyapatite (based on ICDD 9-432).

The degradation process of the scaffolds containing HA NPs was again evaluated following the mass swelling and mass loss ratio profiles [20]. The swelling ratio profiles (Fig. 6a,b) for scaffolds with low HA NPs content (0.5 and 1 wt.%) experience mass swelling and mass loss approximately similar to HA NPs-free scaffold (F2), While, scaffolds with higher (2-5 wt.%) HA NPs show lower mass swelling and mass loss than that HA NPs free, especially at day1. All scaffolds were completely degraded by day14. Scaffolds with 3% HA NPs, showed the lowest mass swelling and mass loss compared to HA NPs- free and to other HA NPs formulations. It showed initial reduction in mass loss but then a slower degradability until it completely degrades at day 21. Day by day analysis of degradation is needed to reveal if there is a difference in the degradation between formulations with HA NPs between days 7 to 14.

Finally, cell viability of the cell-laden scaffolds with different HA NPs contents was studied over a period of 21 days. Figure (7a) shows that cell viability 3 days after incubation is higher (80-90%) for the scaffolds containing HA NPs in the range 1-5 wt.%. Moreover, cell viability increases up to near 100% just 7 days after incubation. It is remarkable that cell viability is higher and circularity is less when HA NPs are present into the scaffold. It is attributed to the fact that hydroxyapatite helps the adhesion and proliferation of cells to the scaffold. Summarizing, Scaffolds containing HA NPs had better cell viability than those without hydroxyapatite. Analysis of cell circularity revealed that cells were less circular (0.4-0.6) at the beginning of the culture at day 3, while they became more circular (0.6-0.8) during the proceeding

days (day 7, 14 and 21). That could be attributed to the

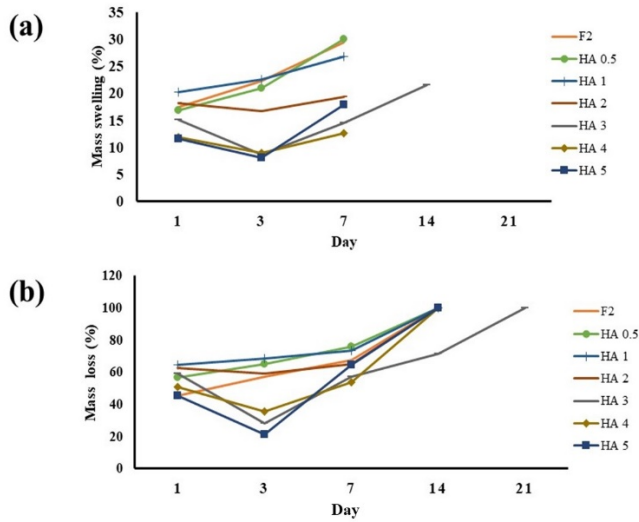


Fig. 6 (a) mass swelling and (b) mass loss ratio profiles for the scaffolds containing variable amounts of HA NPs.

degradation of the scaffolds and the leakage of the HA NPs as they are not chemically attached to the alginate chains. Compared to formulations without HA NPs the circularity was lower at the beginning of the culture (cells are more flat), due to the effect of HA NPs which is a natural component of normal bone enhances cell attachment.

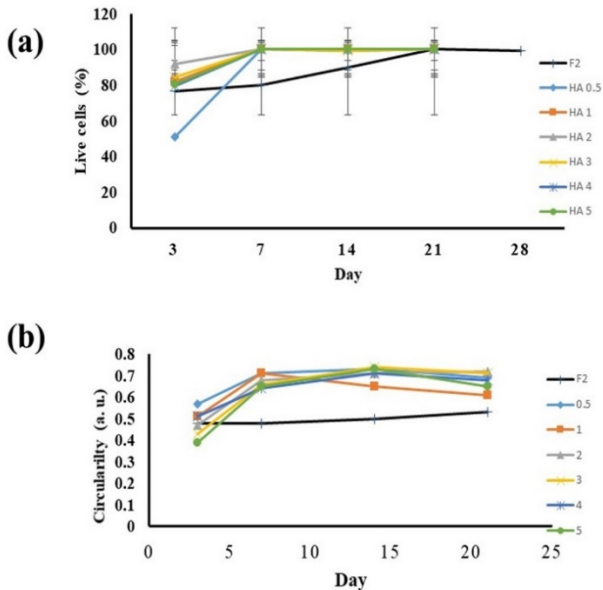


Fig. 7. Graphs showing (a) live cells percentage in scaffolds of alginates with HANP. (b) Circularity of cells in scaffolds of alginates with HANP.

The analysis of the cell morphology show that more oval cells (type ii) (Fig. 3c, middle) than rounded cells were seen in the early days of culture (days 3 and 7), while more rounded cells were observed by the end of the culture which agrees with the circularity analyses. Cells became less in number and in size at days 14 and 21, which might be due to scaffolds degradation and the wash out of unattached cells. No cell of type i was observed, cells had a distinctive oval shape with acentric nucleus (Fig. 3c, middle). Cells in formulation HA3% were more abundant than the rest of the formulations with HANPs because of the longer degradation time.

## V. CONCLUSION

All formulations were printable with acceptable degradation rate except for F1 which was very fragile, although it showed the best viability and bigger size of cells especially at the beginning of the culture but because of fast degradation, cells couldn't attach or divide at the end of the culture. Other formulations without HANPs showed varied degradation and viability the best was F2 compromising with the stiffness, F5 showed better viability and cell attachment at the end of the culture due to less degradation. On the other hand, scaffolds with HANPs, all formulations were printable, 0.5 and 1% HA NPs showed mass swelling and mass loss similar to F2, which shares the same percentage of alginates, while, formulation with higher content of HA NPs showed less mass swelling and mass loss. In terms of viability, better viability rates as well as circularity compared to scaffolds without HA NPs was observed at the early days of culture. But no big difference in viability or cell was observed between the 6 formulations, by the end of the culture cells were more circular. The variety of scaffolds combination gives different alternatives for application in tissue engineering according to the needed tissue graft stiffness and degradation especially that all of them retained approximately 100% living cells after 28 days of culture. It is worth mentioning that the pore size besides the degradation and the scaffolds stiffness may play a major role in the growth and attachment of cells.

More research should be done using different types of stem cells. Viability and division of cells should be evaluated using metabolism assay rather than visual estimation. More control of the percentage of live/dead cells should be done for cells before the printing process. Pore size analysis compared to cell size, mechanical and rheological tests are suggested to be done to the different formulations as they might have an influence on the cell proliferation.

## IV. REFERENCES

- [1] C. Castells-Sala, M. Alemany-Ribes, T. Fernández-Muñoz, L. Recha-Sancho, P. López-Chicón, C. Aloy-Reverté, J. Caballero-Camino, A. Márquez-Gil and C. E. Semino. Current Applications of Tissue Engineering in Biomedicine. J Biochip Tissue chip S2:004.
- [2] A. Atala. Tissue engineering of reproductive tissues and organs. fertnstert. July 2012. Volume 98, Issue 1, P. 21–290.

- [3] J. Lee, J. An and C. Chua. Fundamentals and applications of 3D printing for novel materials. *Applied Materials Today*, June 2017, Vol. 7, P. 120-133.
- [4] T. D. Ngoa, A. Kashania, G. Imbalzano, K. T.Q. Nguyen and D. Huib. Additive manufacturing (3D printing): A review of materials, methods, applications and challenges. *Composites Part B* 143, 2018, 172–196.
- [5] S. R. Caliarì and J. A. Burdick. “A practical guide to hydrogels for cell culture” *Nature methods*, May 2016, Vol.13, no.5, P. 405.
- [6] X. Wang, C. Wei, B. Cao, L. Jiang, Y. Hou and J. Chang. “Fabrication of Multiple-Layered Hydrogel Scaffolds with Elaborate Structure and Good Mechanical Properties via 3D Printing and Ionic Reinforcement” *ACS Appl. Mater. Interfaces* 2018, 10, 18338–18350.
- [7] T. Wang, N. He. *Nanoscale*. “Preparation, characterization and applications of low-molecular-weight alginate-oligochitosan nanocapsules”. Feb, 2010, 2(2):230-9.
- [8] A. Barba, A. Diez-Escudero, Y. Maazouz, K. Rappe, M. Espanol, E. B. Montufar, M. Bonany, J. M. Sadowska, J. Guillem-Marti, C. Öhman-Mägi, C. Persson, M. Manzanares, J. Franch and M. Ginebra. “Osteoinduction by Foamed and 3D-Printed Calcium Phosphate Scaffolds: Effect of Nanostructure and Pore Architecture”. *ACS Appl. Mater. Interfaces* 2017, 9, P. 41722–41736.
- [9] J. J. Escobar-Chávez, M. López-Cervantes, A. Naik, Y. N. Kalia, D. Quintanar-Guerrero and A. Anem-Quintanar. “Applications of thermoreversible pluronic f-127 gels in pharmaceutical formulations” *J Pharm Pharmaceut*, 9, 2006, (3): 339-358.
- [10] P. A. Williams, K. T. Campbell, E. A. Silva. “Alginate hydrogels of varied molecular weight distribution enable sustained release of sphingosine-1-phosphate and promote angiogenesis” *Jan*, 2018 Vol. 106A, ISSUE 1, P. 138-146.
- [11] I. Canals, A. Ginisty, E. Quist, R. Timmerman, J. Fritze, G. Miskinyte, E. Monni, M. G. Hansen, I. Hidalgo, D. Bryder, J. Bengzon and H. Ahlenius “Rapid and efficient induction of functional astrocytes from human pluripotent stem cells” *Nature Methods*, 2018, Vol 15, P.693–696.
- [12] M. S. Carvalho, A. A. Poundarik, J. M. S. Cabral, C. L. da Silva and D. Vashishth. “Rapid and efficient induction of functional astrocytes from human pluripotent stem cells” *Nature Methods*, scientific reports, 2018, 8:14388.
- [13] U. Jammalamadaka and K. Tappa. “Review, Recent Advances in Biomaterials for 3D Printing and Tissue Engineering” *J. Funct. Biomater.* 2018, 9, 22.
- [14] G. Scionti, L. Rodriguez-Arco, M. T. Lopez-Lopez, A. L. Medina-Castillo, I. Garzon, M. Alaminos, M. Toledano and R. Osorio. “Effect of functionalized PHEMA micro- and nano-particles on the viscoelastic properties of fibrin-agarose biomaterials” *J Biomed Mater Res A*. 2018 Mar;106(3):738-745.
- [15] S. M. Roca and M. P. Ginebra. Scaffolds of biocompatible hydrogels for tissue engineering through 3d printing. Master thesis, Biomaterials, Biomechanics and Tissue Engineering Research, Barcelona, Spain, UPC. 2016
- [16] A. G. Navas, M. Ginebra and Giuseppe Scionti. “Development and optimization of a novel bio-ink for 3d printing of bioengineered tissues” Master thesis. Department of materials science and metallurgical engineering, UPC, Barcelona, Spain, 2017.
- [17] V. V. M. and M. P. Ginebra. “3d printed scaffolds with core-shell structure for bone tissue engineering” Master thesis, Joint European Master in Advance Materials Science and Engineering, 2017
- [18] S. T. Bendtsen. “Alginate Hydrogels for Bone Tissue Regeneration” Doctoral dissertation, University of Connecticut, 2017.
- [19] Z. Zhao, M. Espanol, J. Guillem-Marti, D. Kempf, A. Diez-Escudero and M.-P. Ginebra. “ Ion-doping as a strategy to modulate hydroxyapatite nanoparticle internalization.” *Nanoscale*, 2016,8, P. 1595-1607.
- [20] K. S. Lim, J. J. Roberts, M. H. Alves, L. A. Poole-Warren and P. J. Martens. “Understanding and tailoring the degradation of PVA-tyramine hydrogels”. *J. Appl. Polym. Sci.* 2015. P.42142.
- [21] N. Sultana and M. Wang, “1PHBV/PLLA-based composite scaffolds fabricated using an emulsion freezing/freezing-drying technique for bone tissue engineering: surface modification and in vitro biological evaluation.” *Biofabrication* 4, 2012, 015003, P.14.
- [22] M. M. Mirhosseini, V. Haddadi-Asl and S.S. Zargarian. “Fabrication and characterization of polymer-ceramic nanocomposites containing pluronic F127 immobilized on hydroxyapatite nanoparticles” *RSC Adv.* 6 (2016), 80564; 2.
- [23] Q. Liu, Q. Li, S. Xu, Q. Zheng, X. Cao, Preparation and properties of 3D printed alginate-chitosan polyion complex hydrogels for tissue engineering, *Polymers*, 10, 2018, 664; 3.
- [24] T. Al Kayal, D. Panetta, B. Canciani, P. Losi, M. Tripodi, S. Burchielli, P. Ottoni, P. A. Salvadori and G. Soldani, “Evaluation of the effect of a gamma irradiated DBM-Pluronic F127 composite on bone regeneration in wistar rat” *PLOS One* 10(4) (2015) e0125110; 4.
- [25] G.A. Naikoo, M. Thomas, M.A. Ganaie, M. Sheikh, M. Bano, I. Hassan and F. Khan. “Hierarchically macroporous silver monoliths using pluronic F127: Facile synthesis, characterization and its application as an efficient biomaterial for pathogens” *J. Saudi Chem. Soc.* 20 (2016) 237.
- [26] S. T. Bendtsen, S. P. Quinnell and M. Wei. “Development of a novel alginate-polyvinyl alcohol-hydroxyapatite hydrogel for 3D bio-printing bone tissue engineered scaffolds” *J Biomed Mater Res A*. 2017 May;105(5):1457-1468.